



Broad compositional tunability of indium tin oxide nanowires grown by the vapor-liquid-solid mechanism

M. Zervos, C. N. Mihailescu, J. Giapintzakis, C. R. Luculescu, N. Florini, Ph. Komninou, J. Kioseoglou, and A. Othonos

Citation: *APL Materials* **2**, 056104 (2014); doi: 10.1063/1.4875457

View online: <http://dx.doi.org/10.1063/1.4875457>

View Table of Contents: <http://scitation.aip.org/content/aip/journal/aplmater/2/5?ver=pdfcov>

Published by the [AIP Publishing](#)

Articles you may be interested in

[Au-free InAs nanowires grown in In-particle-assisted vapor-liquid-solid mode: growth, structure, and electrical property](#)

AIP Advances **3**, 052107 (2013); 10.1063/1.4804542

[Diameter dependent optical emission properties of InAs nanowires grown on Si](#)

Appl. Phys. Lett. **101**, 053103 (2012); 10.1063/1.4739001

[Selective-area vapor-liquid-solid growth of tunable InAsP quantum dots in nanowires](#)

Appl. Phys. Lett. **98**, 251101 (2011); 10.1063/1.3600777

[Doping nanowires grown by the vapor-liquid-solid mechanism](#)

Appl. Phys. Lett. **95**, 063105 (2009); 10.1063/1.3204543

[Raman and photoluminescence properties of highly Cu doped ZnO nanowires fabricated by vapor-liquid-solid process](#)

J. Chem. Phys. **129**, 124713 (2008); 10.1063/1.2981050

CALL FOR PAPERS

AIP | APL Materials

Special Topic on Perovskite Solar Cells
Ground Breaking Research in Power Efficiency

Guest Editors: Henry Snaith & Lukas Schmidt-Mende

SUBMIT BY **MAY 1, 2014**

Broad compositional tunability of indium tin oxide nanowires grown by the vapor-liquid-solid mechanism

M. Zervos,^{1,2,a} C. N. Mihailescu,^{1,2,3} J. Giapintzakis,^{1,2} C. R. Luculescu,^{2,3} N. Florini,⁴ Ph. Komninou,⁴ J. Kioseoglou,⁴ and A. Othonos^{1,5}

¹Nanotechnology Research Centre (NRC), University of Cyprus, P.O. Box 20537, Nicosia 1678, Cyprus

²Department of Mechanical and Manufacturing Engineering, University of Cyprus, P.O. Box 20537, Nicosia 1678, Cyprus

³National Institute for Laser, Plasma and Radiation Physics, Str. Atomistilor, P.O. Box MG-36, 077125 Magurele, Romania

⁴Nanostructured Materials Microscopy Group (NMMG), Department of Physics, Aristotle University of Thessaloniki, GR-54124 Thessaloniki, Greece

⁵Research Center of Ultrafast Science, Department of Physics, University of Cyprus, P.O. Box 20537, Nicosia 1678, Cyprus

(Received 14 March 2014; accepted 28 April 2014; published online 12 May 2014)

Indium tin oxide nanowires were grown by the reaction of In and Sn with O₂ at 800 °C via the vapor-liquid-solid mechanism on 1 nm Au/Si(001). We obtain Sn doped In₂O₃ nanowires having a cubic bixbyite crystal structure by using In:Sn source weight ratios > 1:9 while below this we observe the emergence of tetragonal rutile SnO₂ and suppression of In₂O₃ permitting compositional and structural tuning from SnO₂ to In₂O₃ which is accompanied by a blue shift of the photoluminescence spectrum and increase in carrier lifetime attributed to a higher crystal quality and Fermi level position. © 2014 Author(s). All article content, except where otherwise noted, is licensed under a Creative Commons Attribution 3.0 Unported License. [<http://dx.doi.org/10.1063/1.4875457>]

Indium tin oxide (ITO) or Sn doped In₂O₃ nanowires (NWs) are important as transparent conducting oxides (TCOs) for the fabrication of solar cells,^{1–3} flexible displays,⁴ and ultra violet light emitting diodes^{5–9} because it has been suggested that higher Sn doping levels and conductivities can be attained in ITO NWs compared to bulk ITO. So far ITO NWs have been grown by carbothermal reduction of In₂O₃ and SnO₂⁵ but the control of stoichiometry is not trivial as it has been observed that SnO₂ NWs may be obtained even when a higher content of In₂O₃ is used during carbothermal reduction carried out under an inert gas flow at elevated temperatures^{10,11} which also leads to the non-intentional incorporation of carbon. In addition ITO NWs have been grown by pulsed laser deposition (PLD) of In₂O₃ and SnO₂ as shown recently by Meng *et al.*¹² Furthermore, ITO NWs have been obtained from the reaction of In and Sn with O₂ by reactive vapor transport as both metals have low melting points of 157 °C and 232 °C, respectively, and similar vapor pressures. For instance, Chiu *et al.*¹³ obtained ITO NWs at 900 °C under a flow of Ar by using 20 nm diameter Au nanoparticles (NPs) on Si(001) and a fixed In:Sn source weight ratio of 9:1 while Chang *et al.*¹⁴ used a fixed In:Sn source weight ratio of 9:1 and obtained ITO NWs on 5 nm Au/Si(001) at 600 °C using Ar, H₂ and O₂. However, despite all of these efforts only few have investigated in detail the incorporation of Sn and the changes that occur in the crystal structure of ITO NWs by changing the In:Sn source ratio over a broad range.^{5,12} For instance, Meng *et al.*¹² obtained 20 at. % Sn in their ITO NWs using PLD by varying the In₂O₃:SnO₂ ratio of their target so that the corresponding Sn:In + Sn at. % ratio was 1%, 5%, 10%, 30%, 50%, and 90%. In contrast, Gao *et al.*⁵ obtained 6.4 at. % Sn in their ITO NWs by varying the SnO₂:In₂O₃: C at. % ratio from 0.05:0.95:1.0 up to 0.6:0.4:1.0.

^aAuthor to whom correspondence should be addressed. Electronic mail: zervos@ucy.ac.cy



Here we have grown ITO NWs on 1 nm Au/Si(001) via the reaction of In and Sn with O₂ at 800 °C and 10⁻¹ mbar by varying systematically the In:In + Sn% weight ratio, hereafter denoted simply as % In, which was equal to 3%, 7%, 9%, 12%, 20%, 60%, 70%, 80%, and 100%. For 3% In, we obtained SnO₂ NWs with a tetragonal rutile crystal structure but between 3% to 9% In, we observe the existence of two distinct phases, i.e., SnO₂ with a tetragonal rutile crystal structure and cubic bixbyite In₂O₃ due to the limited miscibility and different ionic radii of In and Sn. Above 12%, In we observe a complete suppression of the tetragonal rutile crystal structure and obtain Sn doped In₂O₃, i.e., ITO NWs. The incorporation of Sn was confirmed by the systematic shift of the (220) peak of In₂O₃ from $\theta = 30.6^\circ$ to 30.75° with increasing % In but also by energy dispersive x-ray analysis which showed a maximum of 5.9 at. % Sn in the In₂O₃ NWs. We observe a blue shift of the photoluminescence (PL) with increasing % In which is accompanied by an increase in carrier lifetime attributed to an improvement in crystal quality and Fermi level residing closer to the conduction band edge.

ITO NWs were grown using a hot wall, low pressure chemical vapor deposition (LPCVD) reactor consisting of four mass flow controllers and a 1" horizontal quartz tube (QT) installed in a furnace capable of reaching 1200 °C which was fed via a micro flow leak valve that was positioned upstream just after the gas manifold. A chemically resistant, rotary pump capable of reaching 10⁻⁴ mbar was connected downstream. For the growth of ITO NWs, Sn (Aldrich, 2-14 Mesh, 99.9%) and In (Aldrich, Mesh 99.9%) were weighed with an accuracy of ± 1 mg. In all cases, the total weight of the In and Sn was approximately equal to 0.2 g and the % In was 3%, 7%, 9%, 12%, 20%, 60%, 70%, 80%, and 100%. Square p⁺ Si(001) samples having dimensions of ≈ 7 mm \times 7 mm were cleaned in trichloroethylene, methanol, acetone, and isopropanol, rinsed with deionised water and dried with nitrogen. A layer of 1 nm Au was deposited on the clean Si(001) surface after removing the native oxide with HF, rinsing in water and drying with nitrogen. The In and Sn along with the 1 nm Au/p⁺ Si(001) samples were loaded in the 1" QT and pumped down to 10⁻⁴ mBar. Then the 1" QT was purged with 600 sccm of Ar for 10 min at 10⁻¹ mbar after which the temperature was increased to 800 °C at 30 °C/min under the same flow of Ar. Upon reaching 800 °C, a small flow of 10 sccm O₂ was added to the main flow of Ar in order to grow the ITO NWs over 60 min after which the O₂ flow was cut off and the reactor was allowed to cool down slowly over 30 min. The ITO NWs were always removed when the temperature was lower than 100 °C and the 1" QT was changed regularly in order to maintain a clean high temperature zone and avoid contamination. The morphology of the ITO NWs was determined by scanning electron microscopy (SEM) while the phase purity and crystal structure were determined by high-resolution x-ray diffraction (HRXRD) using a SmartLab Rigaku diffractometer with a 9 kW rotating anode and parallel monochromatic beam Cu-K _{α 1} radiation. We used a two bounce (220) \times 2 Ge monochromator in the incident beam with horizontal sample stage and coplanar measurement geometry. Furthermore cross section transmission electron microscopy (XTEM) and high-resolution TEM (HRTEM) observations were carried out in a 200 kV JEOL 2011 electron microscope with a point resolution of 0.194 nm and a spherical aberration coefficient C_s = 0.5 mm. Finally, energy dispersive x-ray analysis (EDX) was carried out using a FEI SEM equipped with an EDX Si(Li) detector from EDAX Inc.

The reaction of Sn with O₂ over the 1 nm Au/Si(001) surface at 800 °C lead to a high yield, uniform growth of SnO₂ NWs with average diameter of ≈ 50 nm and lengths up to 100 μ m which appeared as a white layer. The SnO₂ NWs exhibited clear and well resolved XRD peaks corresponding to the tetragonal rutile crystal structure of SnO₂. This is in agreement with selected area electron diffraction (SAED) pattern and HRTEM analysis carried out previously on SnO₂ NWs obtained using the same growth conditions, which verified that they crystallize in the tetragonal rutile phase belonging to the P42/mnm space group with lattice constants of $a = 0.4738$ nm and $c = 0.3186$ nm.¹⁵ Similarly, the reaction of In and Sn with O₂ over the 1 nm Au/Si(001) using exactly the same growth conditions lead to the growth of ITO NWs with diameters of a few tens of nm's and lengths up to 100 μ m as shown in Fig. 1(a) but they appeared as a light green layer. Here it should be noted that pure In₂O₃ NWs obtained from the reaction of In with O₂ at 800 °C and 1 mBar using a new 1" QT were tapered consistent with the morphology of In₂O₃ NWs obtained previously from the reaction of In and Ar:O₂ at 900 °C and 1 atm.¹⁹ We find that a few % Sn in In resulted into a change in morphology and the growth of NWs like those shown in Fig. 1(a) implying that Sn plays

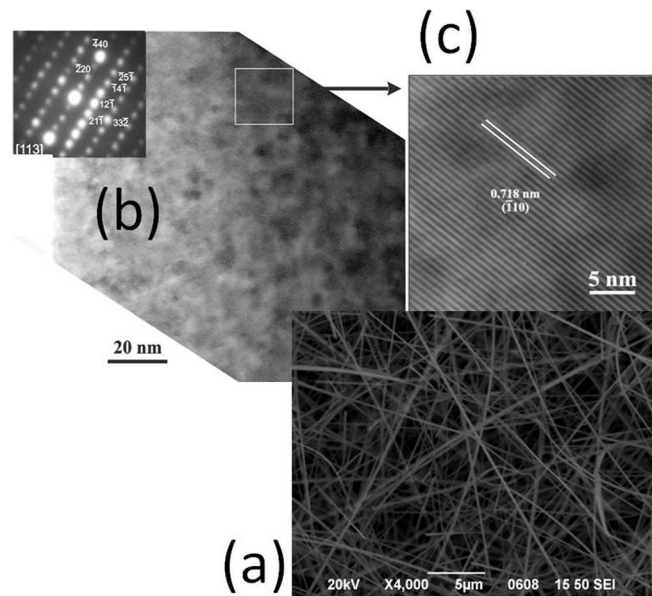


FIG. 1. (a) Typical SEM image of ITO NWs obtained using 20% In. (b) TEM image of ITO NWs obtained using 70% In with diameter of ≈ 100 nm. The growth direction is the (100). (c) Magnified part showing the lattice fringes of the $\{-110\}$ planes of In_2O_3 .

a key role in the growth of ITO NWs. More specifically, we find that the ITO NWs do not grow on plain Si(001) and have spherical NPs on their ends suggesting that they grow by the VLS mechanism consistent with Meng *et al.*¹² who also showed that the Au NP on the end of the ITO NWs is richer in Sn than In.

The high-resolution XRD patterns of the ITO NWs obtained for different % In contents are shown in Fig. 2. More specifically, for 3% In, we observe the formation of SnO_2 NWs with a tetragonal rutile crystal structure but no evidence for the In_2O_3 cubic bixbyite structure. However, for 7% In, we observe the existence of two distinct phases corresponding to the cubic bixbyite crystal structure of In_2O_3 and tetragonal rutile crystal structure of SnO_2 . Interestingly, the (110) dominant reflection of SnO_2 is suppressed when the In content is increased to 9% and disappears at 12% In in which case the XRD peaks show a small shift from those corresponding to the pure In_2O_3 . It should be noted that we do not find any evidence for the existence of SnO , which is a p-type semiconductor. The existence of the tetragonal rutile crystal structure of SnO_2 and cubic bixbyite of In_2O_3 for $< 10\%$ In is attributed to the different ionic radii of Sn^{4+} and In^{3+} , which prevents complete miscibility and leads to phase separation. On the other hand, the shift of the XRD peaks from the cubic bixbyite crystal structure of In_2O_3 above 10% In is due to the incorporation or doping of Sn into the In_2O_3 NWs, i.e., the formation of ITO NWs. A typical TEM image of the ITO NWs obtained for 70% In is shown in Fig. 1(b). The lattice fringe spacing measured from the HRTEM image shown in Fig. 1(c) equals 0.718 nm and corresponds to the d-spacing of the $\{-1,1,0\}$ crystallographic planes of the In_2O_3 cubic bixbyite structure. Nevertheless, it was not possible to determine the distortion of the crystal structure due to the incorporation of Sn from HRTEM. In order to investigate the incorporation of Sn in the In_2O_3 NWs, we have determined the changes that occur in the lattice constant of the In_2O_3 NWs with increasing % In from the shift of the XRD peaks as shown in the inset of Fig. 3. This shift has also been observed in the case of ITO NWs obtained from the carbothermal reduction of In_2O_3 and SnO_2 by Gao *et al.*⁵ The expanded view of the (222) reflection of In_2O_3 depicted as an inset in Fig. 3 shows its dependence on the % In but contradicts Vegard's law which predicts a contraction in the host lattice due to the radius of the Sn^{4+} ion (0.71 Å) which is smaller compared to that of In^{3+} (0.81 Å).⁵ This contradiction has been attributed to the large repulsive force arising from additional positive charges of the Sn cations^{16,17} or to the increase of interstitial O which neutralizes the extra positive charges.¹⁸ The variation of the lattice constant of

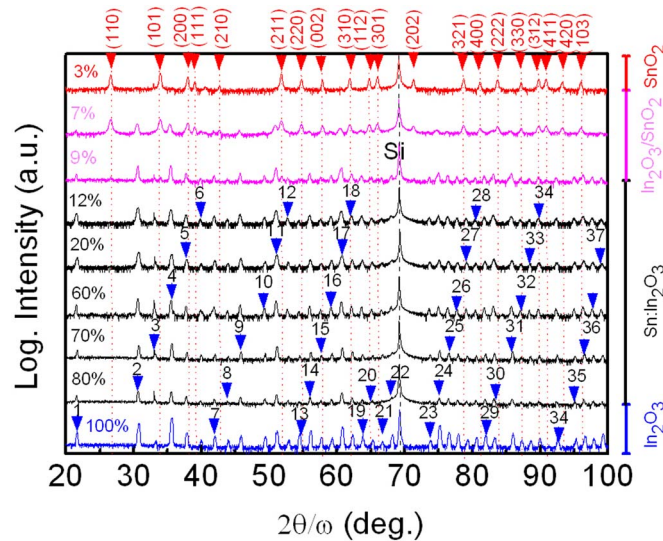


FIG. 2. HXRD patterns of the ITO NWs. The peaks of In_2O_3 (ICDD 04-012-5550) are labeled by arrows and numbers, i.e., 1–37 corresponding to (200), (222), (123), (400), (411), (420), (332), (422), (134), (125), (440), (433), (600), (611), (026), (145), (622), (136), (444), (543), (046), (633), (156), (800), (811), (820), (653), (822), (831), (662), (048), (833), (248), (761), (158), (763), (844), (853), (1000) in ascending order. The peaks of SnO_2 (ICDD 01-071-5323) are given at the top.

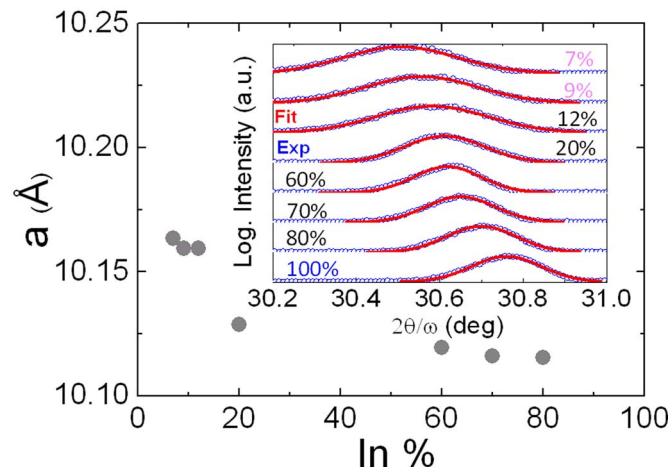


FIG. 3. Variation of the lattice constant of the ITO NWs for different % In. Inset shows high-resolution XRD scans of the (222) diffraction peak of ITO NWs obtained using 100%, 80%, 70%, 60%, 20%, 12%, 9%, 7%, and 3% In.

the ITO NWs with In content determined from the (222) reflection of In_2O_3 is shown in Fig. 3. The lattice constant is 10.065 Å in the case of pure In_2O_3 and reaches a maximum value of 10.1634 Å for 7% In which is accompanied by the appearance of SnO_2 peaks as shown in Fig. 1. In order to verify the incorporation of Sn into the In_2O_3 NWs, we also carried out EDX and the % In and Sn compositions of the ITO NWs are listed as an inset in Fig. 4 along with EDX spectra. For 3% and 7% In, we obtain SnO_2 NWs containing 2.96% and 3.3% In, respectively, corresponding to the existence of two distinct phases in accordance with high-resolution XRD. However, the cubic bixbyite crystal structure of In_2O_3 is dominant for 9% In and we observe a suppression of the tetragonal rutile crystal structure of SnO_2 , which disappears at 12% In in which case we obtain ITO NWs. We find a maximum incorporation of 5.86 wt. % Sn or 3.5 at. % Sn in the In_2O_3 NWs which is closer to the findings of Gao *et al.*⁵

In addition to the structural and compositional tuning of the ITO NWs, we observed a blue shift of the PL with increasing % In as shown in Fig. 5. More specifically we obtain a broad PL with a

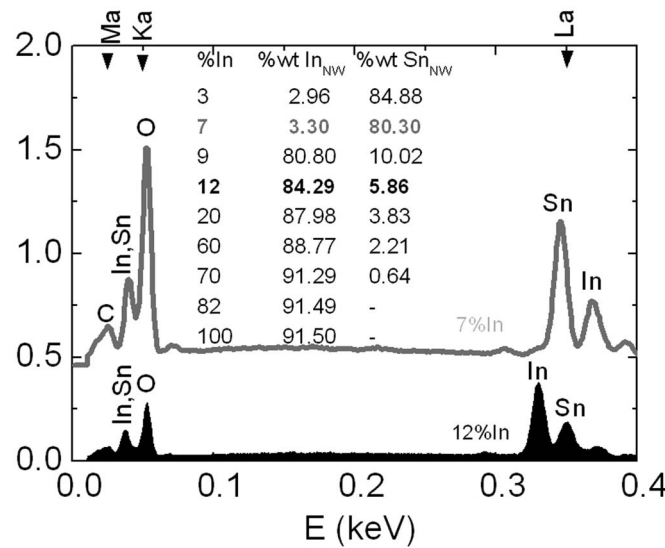


FIG. 4. EDX spectra of the ITO NWs for 7% and 12% In. Also shown as an inset table of % In and Sn in the ITO NWs versus % In in the source of In:Sn.

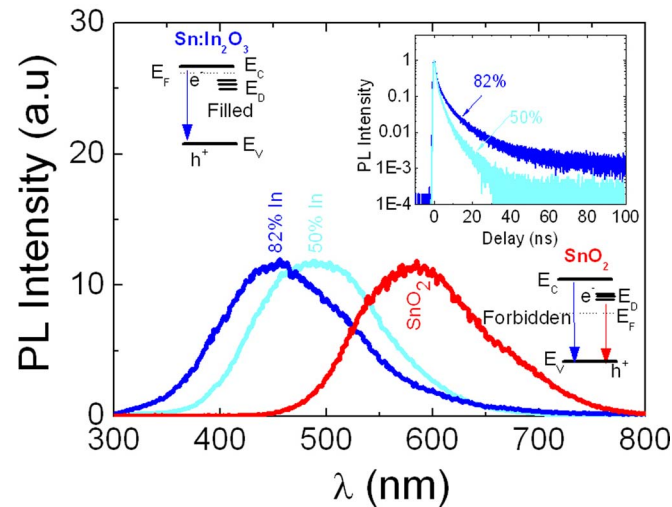


FIG. 5. PL spectra obtained at $T = 300$ K with $\lambda = 266$ nm for SnO_2 NWs and ITO NWs using 50% and 82% In; inset shows the corresponding time resolved PL along with energy band diagrams for the transitions that occur in SnO_2 and $\text{Sn:In}_2\text{O}_3$ NWs.

maximum at $\lambda = 600$ nm (≈ 2.0 eV) from the SnO_2 NWs which shifts to 500 nm (≈ 2.5 eV) for 50% In and to 450 nm (≈ 2.8 eV) for 82% In corresponding to ITO NWs. Besides, we observe an increase in the carrier lifetime as shown by the time resolved PL in the inset of Fig. 5. Before elaborating further, we ought to point out that In_2O_3 is an n-type semiconductor with a direct energy band gap of ≈ 3.5 eV and a lower indirect gap of 2.6 eV. Similarly SnO_2 has a direct energy band gap of 3.7 eV but the even-parity symmetry of the conduction-band minimum and valence-band maximum states prohibits band-edge radiative transitions which has hindered the potential application of SnO_2 as an optoelectronic device. The broad PL of the SnO_2 NWs at ≈ 600 nm or 2.0 eV is due to radiative recombination between defect states that are located energetically in the upper half of the energy band gap and hole states in the valence band as shown schematically in Fig. 5 and as we have shown using ultrafast time resolved absorption transmission spectroscopy not only in SnO_2 but also in In_2O_3 NWs.¹⁹ We suggest that the shift of the PL maximum from 2.0 to 2.8 eV with increasing

% In and the increase in carrier lifetime is attributed to an improvement in crystal quality and the position of the Fermi level which resides close to the conduction band as a result of doping with Sn.

ITO NWs have been grown over a broad range of compositions via the reaction of high purity In and Sn with O₂ on 1nmAu/Si(001) at 800 °C and 10⁻¹ mBar by varying systematically the % In in the source of In:Sn from 10% to 100%. The ITO NWs had diameters of 50 nm and lengths up to 100 μm and the incorporation of Sn in the In₂O₃ NWs was confirmed by the systematic shift of the (220) peak of In₂O₃ from $\theta = 30.6^\circ$ to 30.75° but also by EDX analysis which showed that a maximum of 5.9 wt. % or 3.5 at. % Sn was obtained in the ITO NWs. In contrast, we observed the existence of two distinct phases, i.e., SnO₂ with a tetragonal rutile crystal structure and cubic bixbyite In₂O₃ for 6% to 9% In attributed to the limited miscibility and different ionic radii of In and Sn. Pure like SnO₂ NWs were obtained when a few % In were included in Sn. The blue shift of the PL maximum from 2.0 to 2.8 eV is accompanied by an increase in carrier lifetime attributed to an improvement of crystal quality and the Fermi level which moves closer to the conduction band edge upon increasing the % In.

This work was supported in part by the *Research Promotion Foundation of Cyprus*, project ANAVATHMISI/0609/06.

- ¹ S. Ngamsinlapasathian, T. Sreethawong, Y. Suzuki, and S. Yoshikawa, *Sol. Energy Mater. Sol. Cells* **90**, 2129 (2006).
- ² R. Hyam, R. K. Bhosale, W. Lee, S. H. Han, and B. Hannoyer, *J. Nanosci. Nanotechnol.* **10**, 5894 (2010).
- ³ A. Hichou, M. Addou, M. Mansori, and J. Ebothé, *Sol. Energy Mater. Sol. Cells* **93**, 609 (2009).
- ⁴ Q. Wan, P. Feng, and T. H. Wang, *Appl. Phys. Lett.* **89**, 123102 (2006).
- ⁵ J. Gao, R. Chen, D. H. Li, L. Jiang, J. C. Ye, X. C. Ma, and X. D. Chen, *Nanotechnology* **22**, 195706 (2011).
- ⁶ Y. Y. Kee, S. S. Tan, T. K. Yong, C. H. Nee, S. S. Yap, T. Y. Tou, G. Sáfrán, Z. E. Horváth, J. P. Moscatello, and Y. K. Yap, *Nanotechnology* **23**, 025706 (2012).
- ⁷ C. O'Dwyer, M. Szachowicz, G. Visimberga, V. Lavayen, S. B. Newcomb, and C. M. S. Torres, *Nat. Nanotechnol.* **4**, 239 (2009).
- ⁸ H. K. Yu, W. J. Dong, G. H. Jung, and J. L. Lee, *ACS Nano* **5**, 8026 (2011).
- ⁹ N. Horiuchi, *Nat. Photonics* **5**, 332 (2011).
- ¹⁰ M. O. Orlandi, R. Aguiar, A. C. Lanfredi, E. Longo, J. A. Varela, and E. R. Leite, *Appl. Phys. A.* **80**, 23 (2005).
- ¹¹ P. Nguyen, H. T. Ng, J. Kong, A. M. Cassell, R. Quinn, J. Li, J. Han, and M. Neil, *Nano Lett.* **3**, 925 (2003).
- ¹² G. Meng, T. Yanagida, K. Nagashima, H. Yoshida, M. Kanai, A. Klamchuen, F. Zhuge, Y. He, S. Rahong, X. Fang, S. Takeda, and T. Kawai, *J. Am. Chem. Soc.* **135**, 7033 (2013).
- ¹³ S. P. Chiu, H. F. Chung, Y. H. Lin, J. J. Kai, F. R. Chen, and J. J. Lin, *Nanotechnology* **20**, 105203 (2009).
- ¹⁴ W. C. Chang, C. H. Kuo, C. C. Juan, P. J. Lee, Y. L. Chueh, and S. J. Lin, *Nanoscale Res. Lett.* **7**, 684 (2012).
- ¹⁵ M. Zervos, A. Othonos, D. Tsokkou, J. Kioseoglou, E. Pavlidou, and Ph. Komninou, *Phys. Status Solidi A* **210**, 226 (2013).
- ¹⁶ G. B. Gonzales, J. B. Cohen, J. H. Hwang, T. O. Mason, J. P. Hodges, and J. D. Jorgensen, *J. Appl. Phys.* **89**, 2550 (2001).
- ¹⁷ G. Neri, A. Bonavita, G. Micali, G. Rizzo, N. Pinna, M. Niderberger, and J. Ba, *Thin Solid Films* **515**, 8637 (2007).
- ¹⁸ G. Frank and H. Kostlin, *Appl. Phys. A.* **27**, 197 (1982).
- ¹⁹ D. Tsokou, M. Zervos, and A. Othonos, *J. Appl. Phys.* **106**, 084307 (2009).